Nanoparticle composite TPNT1 is effective against SARS-CoV-2 and influenza viruses

Sui-Yuan Chang

National Taiwan University College of Medicine

Kuo-Yen Huang

Institute of Biomedical Sciences, Academia Sinica

Tai-Ling Chao

National Taiwan University College of Medicine

Han-Chieh Kao

National Taiwan University College of Medicine

Yu-Hao Pang

National Taiwan University College of Medicine

Lin Lu

Tripod Nano Technology

Chun-Lun Chiu

Tripod Nano Technology

Hsin-Chang Huang

Tripod Nano Technology

Ting-Jen Rachel Cheng

The Genomics Research Center, Academia Sinica

Jim-Min Fang (✉ jmfang@ntu.edu.tw)

The Genomics Research Center, Academia Sinica

Pan-Chyr Yang (✉ pcyang@ntu.edu.tw)

National Taiwan University Hospital and National Taiwan University College of Medicine

---

Research Article

Abstract

A metal nanoparticle composite TPNT1, which contains Au-NP (1 ppm), Ag-NP (5 ppm), ZnO-NP (60 ppm) and ClO_2 (42.5 ppm) in aqueous solution was prepared and characterized by spectroscopy, transmission electron microscopy, dynamic light scattering analysis and potentiometric titration. Based on the in vitro cell-based assay, TPNT1 can inhibit six major clades of SARS-CoV-2 with effective concentration within the range to be used as food additives. TPNT1 was shown to block viral entry by inhibiting the binding of SARS-CoV-2 spike proteins to ACE2 receptor and to interfere with the syncytium formation. In addition, TPNT1 also effectively reduced the cytopathic effects induced by human (H1N1) and avian (H5N1) influenza viruses, including the wild-type and Tamiflu-resistant virus isolates. Together with previously demonstrated efficacy as antimicrobials, TPNT1 can block viral entry and inhibit or prevent viral infection to provide prophylactic effects against both SARS-CoV-2 and opportunistic infections.

Introduction

The ongoing COVID-19 pandemic has imposed on tremendous threat to humans and global socioeconomics. Many researchers have exerted great efforts to develop effective vaccines and drugs against SARS-CoV-2, the causative virus of COVID-19. Re-purposing of the existing broad-spectrum antiviral agents for COVID-19 therapeutics [1,2], including remdesivir, favipiravir, lopinavir and hydroxychloroquine, has been reported to inhibit SARS-CoV-2 based on the in vitro assays. Remdesivir is even recently applied in compassionate use for patients with severe COVID-19 infection [3]. In contrast to the small molecules, we consider using metal nanoparticles as the prophylactic of COVID-19 infection. Silver nanoparticle (Ag-NP) and zinc oxide nanoparticle (ZnO-NP) are well-known antimicrobial agents against many kinds of bacteria, fungi and viruses [4,5]. Gold nanoparticle (Au-NP) also shows potential use in suppressing human immunodeficiency virus and *Mycobacterium tuberculosis* bacteria [6].

Results

In this study, we formulated a metal nanoparticle composite TPNT1, which contains Au-NP (1 ppm), Ag-NP (5 ppm), ZnO-NP (60 ppm) and ClO_2 (42.5 ppm) in aqueous solution with a positive zeta potential of +32.81 mV. The individual metal nanoparticles were synthesized according to our patented method [7]. In brief, a metal aqueous solution ($HAuCl_4$, $AgNO_3$ or $ZnCl_2$) was reduced by heating with citric acid at 150 ^oC for 12 min, and then dispersed in an appropriate medium to obtain the colloidal metal nanoparticles. The physicochemical properties of the synthesized nanoparticles were fully characterized (Figure S1) by ultraviolet-visible spectroscopy, infrared spectroscopy, inductively coupled plasma atomic emission spectroscopy, transmission electron microscopy (TEM), dynamic light scattering (DLS) analysis and potentiometric titration. According to the TEM imaging, Au-NP, Ag-NP and ZnO-NP are in spherical shape with 20−40, 10−40 and 25−35 nm diameters, respectively. The average sizes of colloidal Au-NP, Ag-NP and ZnO-NP are 78.1, 50.4 and 619.1 nm as shown by the DLS analysis, respectively.

The antiviral activity of TPNT1 against SARS-CoV-2 was first examined by plaque reduction assay. Briefly, Vero E6 cells were infected with SAR-CoV-2 (BetaCoV/Taiwan/NTU01/2020) in the presence of various concentrations of the TPNT1. As shown in Figure 1A, an obvious reduction of plaque numbers and sizes was observed in the presence of 100-fold diluted TPNT1. The calculated IC_{50} for TPNT1 is 143±15.5-fold dilution (containing 0.71±0.08 ppm Au-NP, 0.71±0.08 ppm Ag-NP, 1.77±0.2 ppm ZnO-NP, and 1.2±0.14 ppm ClO_2). Yield reduction assay was subsequently performed to determine the antiviral activity of TPNT1 by either pretreating the virus with TPNT1 (pretreat + infection), adding TPNT1 during (infection) or after virus infection (post-infection). The schematic illustration for experimental design was shown in Figure 1B. Twenty-four hours after infection, cytopathic effects (CPE) was observed in virus infected cells without pretreatment of virus with TPNT1, and in the infection and post-infection group with or without TPNT1 treatment (Figure S2A). The culture supernatants and cell lysates were harvested for subsequent analysis. The virus copy number in the culture supernatant was determined by quantitative real-time RT-PCR (qRT-PCR) (Figure 1C). The replication of virus in the infected cells was determined by quantification of intracellular viral mRNA and viral nucleocapsid protein (NP) expression using the qRT-PCR of oligo-dT amplified cDNA (Figure 1D), western blot analysis (Figure 1E), and immunofluorescence assay (Figure 1F). Based on the experimental results, pre-incubation of diluted TPNT1 with SARS-CoV-2 is required for efficient inhibition of the virus replication. TPNT1 functioned at a stage before virus infection since the virus titers in the supernatants reduced significantly when TPNT1 was preincubated with virus before infection (Figure 1C). Corresponding reduction of intracellular viral RNA and viral NP protein expression was only observed in cells infected with TPNT1-pretreated viruses (Figure 1D−F). No cell toxicity was observed based on the acid phosphatase (ACP) assay (Figure S2B). The selectivity index (CC_{50}/IC_{50}) was greater than 10.

The ability of TPNT1 to inhibit binding of angiotensin-converting enzyme 2 (ACE2) to SARS- CoV-2 receptor was also confirmed by the ELISA assay using ACE2-Fc-Biotin and spike protein. As shown in Figure 2A, TPNT1 can block binding of spike protein to ACE2-Fc-Biotin in a dose- dependent manner. Furthermore, such inhibition was shown to interfere with the syncytium formation between 293T/Spike/EGFP and H1975-ACE2 cells (Figure 2B) under an inverted fluorescence microscope. A significant inhibition of syncytium formation was demonstrated in the presence of TPNT1 as compared to the solvent (H_2O) control (Figure 2C). Finally, the ability of TPNT1 to inhibit various SARS-CoV-2 was demonstrated using 6 clinical isolates representing 6 major clades of SARS-CoV-2 viruses. As shown in Figure S3, viral RNA in the culture supernatants and cell extracts was significantly inhibited in the presence of TPNT1.

In addition to SARS-CoV-2, we also tested the activities of TPNT1 against influenza virus infection in cell-based assays. Influenza virus infects millions of people annually and can cause severe diseases, especially in elderly [8]. Although there are several drugs to treat flu clinically, drug-resistant viruses have quickly emerged and thus new therapeutics targeting drug-resistant viruses are needed [9]. We therefore tested the antiviral activities of TNPT1 against influenza virus. The results showed that TNPT1 effectively relieved the cells with virus-induced toxicity (Figure 3). The effects of TNPT1 did decrease slightly when

the cells were infected with extremely high viral loads. Nonetheless, the protection of TNPT1 on the CPE of infected cells is remarkable. In addition, the activities of TNPT1 were detected in the cells infected with wild-type drug- sensitive strains (Figure 3A and 3C) as well as the drug-resistant strains (Figure 3B and 3D) that have H274Y mutation accounting for resistance towards oseltamivir (Tamiflu[TM]).

Discussion

Receptor binding is critical for viral entry and subsequent virus replication in host cells. SARS-CoV-2 uses its spike protein to interact with the ACE2 receptor on host cells to facilitate virus entry and infection [10,11]. The hemagglutinin (HA) of avian and human influenza viruses is responsible to bind the 2,3-linked or 2,6-linked Neu5Ac receptor on host cells [12]. The SARS- CoV-2 and influenza virions having average diameters of 80−120 nm are in the size range of nanoparticles. As TPNT1 is most effective by pre-incubation with viruses, one possible mechanism for the antiviral activity of TPNT1 may be attributable to bindings of virus surface glycoproteins with the metal nanoparticles, and thus preventing the virions from attachment to host cells [13,14]. Indeed, our experiments (Figure 2) support that TPNT1 can block viral entry by inhibiting the binding of SARS-CoV-2 spike proteins to ACE2 receptor and to interfere with the syncytium formation. It is suggested that nanoparticles can interact with the sulfur-bearing residues on the viral surface. For example, SARS-CoV-2 spike has 40 cysteine residues while influenza hemagglutinin has 15 cysteine residues. Those residues can easily bind to the metal nanoparticles and the virus entry through these surface proteins would be diminished [15]. Moreover, TPNT1 has positive surface charge (+32.81 mV) that may also enhance the binding with virions [16].

Inclusion of ClO_2 as an oxidizing agent in TPNT1 nanometal composite is beneficial for virus inhibition. A previous report [17] indicates that magnesium oxide nanoparticle (MgO-NP) impregnated with Cl_2 exhibits higher bactericidal activity than free Cl_2 or MgO-NP itself. Another study [18] shows that the combination of single-wall carbon nanotubes and NaOCl (or H_2O_2) also displays a synergistic sporicidal effect. We assume that the ClO_2 component in TPNT1 may render oxidative damage of virus surface, and thus provide enhanced effect for viral inhibition by the metal nanoparticles.

Although metal nanoparticles have been demonstrated to have a wide range of biomedical applications [19], their toxicity is an issue of concern. The degree of toxicity varies by the type, shape, size, purity, concentration, administration method and exposure time of metal nanoparticles. The current available data from many research teams are insufficient, and some are even contradictory, to determine the adverse effects of metal nanoparticles on human health [20,21]. In this study, all the Au-NP, Ag-NP and ZnO-NP in TPNT1 are prepared in spherical form. In general, spherical metal nanoparticles are non-toxic or less toxic than that in other shapes [22]. The amounts of Au-NP (< 1 ppm), Ag-NP (< 1 ppm) and ZnO-NP (< 2 ppm) in the effective dose of TPNT1 tests are within the range of concentration to be used as food additives. The content of ClO_2 (< 1.5 ppm) is also within the safety concentration in drinking water [23].

Both COVID-19 and influenza are severe infectious diseases. In this study, we have shown that TPNT1 is effective in inhibition of SARS-CoV-2 and influenza viruses, including avian H5N1, human H1N1 and the oseltamivir-resistant H274Y strain. Compared with organic drugs, TPNT1 based on inorganic metal nanoparticles will have low tendency to induce resistant viruses. TPNT1 can also provide prophylactic effects against SARS-CoV-2 and opportunistic infections which are frequently observed in patients suffering SARS-CoV-2 infection by oral gargling, nasal spray, nebulized inhalation or even systemic use after an appropriate clinical trial.

Materials And Methods

Characterization of nanoparticles

All the reagents were reagent grade and used as purchase without further purification. Tetrachloroauric acid (HAuCl$_4$, 0.2 M aqueous solution) and zinc powder were purchased from Acros Organics (New Jersey, USA). Silver nitrate (AgNO$_3$, 0.1 M aqueous solution) was purchased from Merck & Co. (New Jersey, USA). Ultra-pure water was purchased from Hao Feng Biotech Co. (Taipei, Taiwan). Particle size distribution and zeta potential were measured on Otsuka ELSZ-2000ZS dynamic light scattering detector.

Antiviral activities against SARS-CoV-2

The clinical isolate of SARS-CoV-2 was named as SARS-CoV-2/NTU01/TWN/human/2020 (PubMed accession MT066175). Plaque reduction assay was performed in triplicate in 24-well tissue culture plates. SARS-CoV-2 was incubated with TPNT1 for 1 h at 37 °C before adding to the cell monolayer for another one hour. Subsequently, virus-TPNT1 mixtures were removed and the cell monolayer was washed once with PBS before covering with media containing 1% methylcellulose for 5–7 days. The cells were fixed with 10% formaldehyde overnight. After removal of overlay media, the cells were stained with 0.7% crystal violet and the plaques were counted.

ACE2-Fc-Biotin and spike binding by ELISA assay

Fifty microliter of 50 ng/mL purified 1-674 spike proteins were pre-coated on to the 96- well ELISA plate at 4 °C overnight. The plate was first washed three times with PBST (PBS containing 0.05% Tween-20) and blocked with blocking buffer (1% BSA, 0.05% NaN$_3$ and 5% sucrose in PBS) at room temperature for 30 min. After that, the plate was washed three times with PBST. Serially diluted ACE2-Fc-Biotin with or without TPNT1 were pre-incubated at 37°C for 1 h. After that, the mixture was added to the 96-well plate and incubated at 37 °C for 1 h. After that, the plate was washed three time with PBST and incubated with horseradish peroxidase (HRP)-conjugated streptavidin (1:500) at 37 °C for 30 min. After three-times wash with PBST, tetramethylbenzidine substrate (TMB) (T8665, Sigma) was added for 30 min before stopping the reaction by 50 μL of 1 N H$_2$SO$_4$. HRP activity was measured at 450 nm using ELISA plate reader (VERSAMAX).

Syncytia formation

HEK293T cells were co-transfected with plasmid 5 μg pCR3.1-Spike and 0.5 μg pLKO AS2-GFP by lipofetamine 3000 (ThermoFisher, L3000015) for three days before use as effector cells (293T-S). H1975 lung adenocarcinoma cells were transduced with lentivirus encoding full length ACE2 before use as target cells (H1975-ACE2). H1975 and H1975-ACE2 were (2×10^5) cultured in RPMI containing 10% FBS at 37 ^{o}C for 24 h. 293T-S cells were detached with 0.48 mM EDTA for 5 min. 293T-S (1×10^5) were incubated with H_2O or TPNT1 at 37 ^{o}C for 1 h. After that, the mixture of TPNT1 and effector cells was added to target cells and incubated at 37 ^{o}C for 24 h. The cells were fixed with 4% paraformaldehyde at room temperature for 30 min. The 293T/Spike/EGFP cells fused or unfused with H1975-ACE2 cells were counted under an inverted fluorescence microscope (Leica DMI 6000B fluorescence microscope). The percent inhibition of syncytia formation was calculated using the following formula: $(100 - (H - L)/(E - L) \times 100)$. H represents the total green fluorescent score in the individual L represents the green fluorescent score in the negative control group with H1975-ACE2 replaced by H1975 as the target cells. E represents the green fluorescent score in each picture in TPNT1 group.

Determination of anti-influenza activities

Recombinant virus Influenza A/WSN/1933 (H1N1), Influenza A/WSN/1933 (H1N1) (NA H274Y), Influenza NIBRG14 (H5N1) harboring the hemagglutinin and neuraminidase from A/Viet Nam/1194/2004 (H5N1) (NA wt), Influenza NIBRG14 (H5N1) (NA H274Y) were produced by using plasmids provided by Dr. King-Song Jeng (Institute of Molecular Biology, Academia Sinica). Influenza virus at indicated titers was mixed with TPNT1 at various dilutions for 1 h at room temperature. The mixtures were used to infect MDCK cells at 1×10^5 cells/mL in 96 wells. After 48 h of incubation at 37 °C under 5% CO_2, the cytopathic effects were determined with CellTiter 96 AQueous Non-Radioactive Cell Proliferation Assay reagent (Promega).

Declarations

Author contributions

SYC, , JMF, and PCY are responsible for experimental design and manuscript writing. KYH, TLC, HCK, YHP, and TJRC conducted most of the experiments. LL, CLC and HCH prepared and characterized TPNT1 for testing.

Transparency declarations

The authors declare no competing financial interest.

References

1 Dong, L., Hu, S. & Gao, J. Discovering drugs to treat coronavirus disease 2019 (COVID- 19). Drug Discoveries & Therapeutics 14, 58-60 (2020).

2 Hu, T. Y., Frieman, M. & Wolfram, J. Insights from nanomedicine into chloroquine efficacy against COVID-19. Nature nanotechnology 15, 247-249, doi:10.1038/s41565- 020-0674-9 (2020).

3 Grein, J. et al. Compassionate Use of Remdesivir for Patients with Severe Covid-19. The New England journal of medicine, doi:10.1056/NEJMoa2007016 (2020).

4 Galdiero, S. et al. Silver nanoparticles as potential antiviral agents. Molecules 16, 8894- 8918, doi:10.3390/molecules16108894 (2011).

5 Rai, M., Ingle, A. P., Birla, S., Yadav, A. & Santos, C. A. Strategic role of selected noble metal nanoparticles in medicine. Critical reviews in microbiology 42, 696-719, doi:10.3109/1040841X.2015.1018131 (2016).

6 Cagno, V. et al. Broad-spectrum non-toxic antiviral nanoparticles with a virucidal inhibition mechanism. Nature materials 17, 195-203, doi:10.1038/nmat5053 (2018).

7 Lu, L. et al. USA patent (2018).

8 Dunning, J., Thwaites, R. S. & Openshaw, P. J. M. Seasonal and pandemic influenza: 100 years of progress, still much to learn. Mucosal immunology, doi:10.1038/s41385-020- 0287-5 (2020).

9 Kormuth, K. A. & Lakdawala, S. S. Emerging antiviral resistance. Nature microbiology 5, 4-5, doi:10.1038/s41564-019-0639-7 (2020).

10 Zhou, P. et al. A pneumonia outbreak associated with a new coronavirus of probable bat origin. Nature 579, 270-273, doi:10.1038/s41586-020-2012-7 (2020).

11 Hoffmann, M. et al. SARS-CoV-2 Cell Entry Depends on ACE2 and TMPRSS2 and Is Blocked by a Clinically Proven Protease Inhibitor. Cell 181, 271-280 e278, doi:10.1016/j.cell.2020.02.052 (2020).

12 Rossman, J. S. & Lamb, R. A. Influenza virus assembly and budding. Virology 411, 229- 236, doi:10.1016/j.virol.2010.12.003 (2011).

13 Mori, Y. et al. Antiviral activity of silver nanoparticle/chitosan composites against H1N1 influenza A virus. Nanoscale research letters 8, 93, doi:10.1186/1556-276X-8-93 (2013).

14 Ghaffari, H. et al. Inhibition of H1N1 influenza virus infection by zinc oxide nanoparticles: another emerging application of nanomedicine. Journal of biomedical science 26, 70, doi:10.1186/s12929-019-0563-4 (2019).

15 Kim, J. et al. Porous gold nanoparticles for attenuating infectivity of influenza A virus. Journal of Nanobiotechnology 18 (2020).

16 Arakha, M., Saleem, M., Mallick, B. C. & Jha, S. The effects of interfacial potential on antimicrobial propensity of ZnO nanoparticle. Scientific reports 5, 9578, doi:10.1038/srep09578 (2015).

17 Stoimenov, P. K., Klinger, R. L., Marchin, G. L. & Klabunde, K. J. Metal Oxide Nanoparticles as Bactericidal Agents. Langmuir 18, 6679−6686 (2002).

18 Lilly, M., Dong, X., McCoy, E. & Yang, L. Inactivation of Bacillus anthracis spores by single-walled

carbon nanotubes coupled with oxidizing antimicrobial chemicals. Environmental science & technology 46, 13417-13424, doi:10.1021/es303955k (2012).

19 Yamada, M., Foote, M. & Prow, T. W. Therapeutic gold, silver, and platinum nanoparticles. Wiley interdisciplinary reviews. Nanomedicine and nanobiotechnology 7, 428-445, doi:10.1002/wnan.1322 (2015).

20 Yahyaei, B., Nouri, M., Bakherad, S., Hassani, M. & Pourali, P. Effects of biologically produced gold nanoparticles: toxicity assessment in different rat organs after intraperitoneal injection. AMB Express 9, 38, doi:10.1186/s13568-019-0762-0 (2019).

21 Meng, J., Zhou, X., Yang, J., Qu, X. & Cui, S. Exposure to low dose ZnO nanoparticles induces hyperproliferation and malignant transformation through activating the CXCR2/NF-kappaB/STAT3/ERK and AKT pathways in colonic mucosal cells. Environmental pollution 263, 114578, doi:10.1016/j.envpol.2020.114578 (2020).

22 Murphy, C. J. et al. Gold nanoparticles in biology: beyond toxicity to cellular imaging. Accounts of chemical research 41, 1721-1730, doi:10.1021/ar800035u (2008).

23 Ma, J. W. et al. Efficacy and Safety Evaluation of a Chlorine Dioxide Solution. International journal of environmental research and public health 14, doi:10.3390/ijerph14030329 (2017).
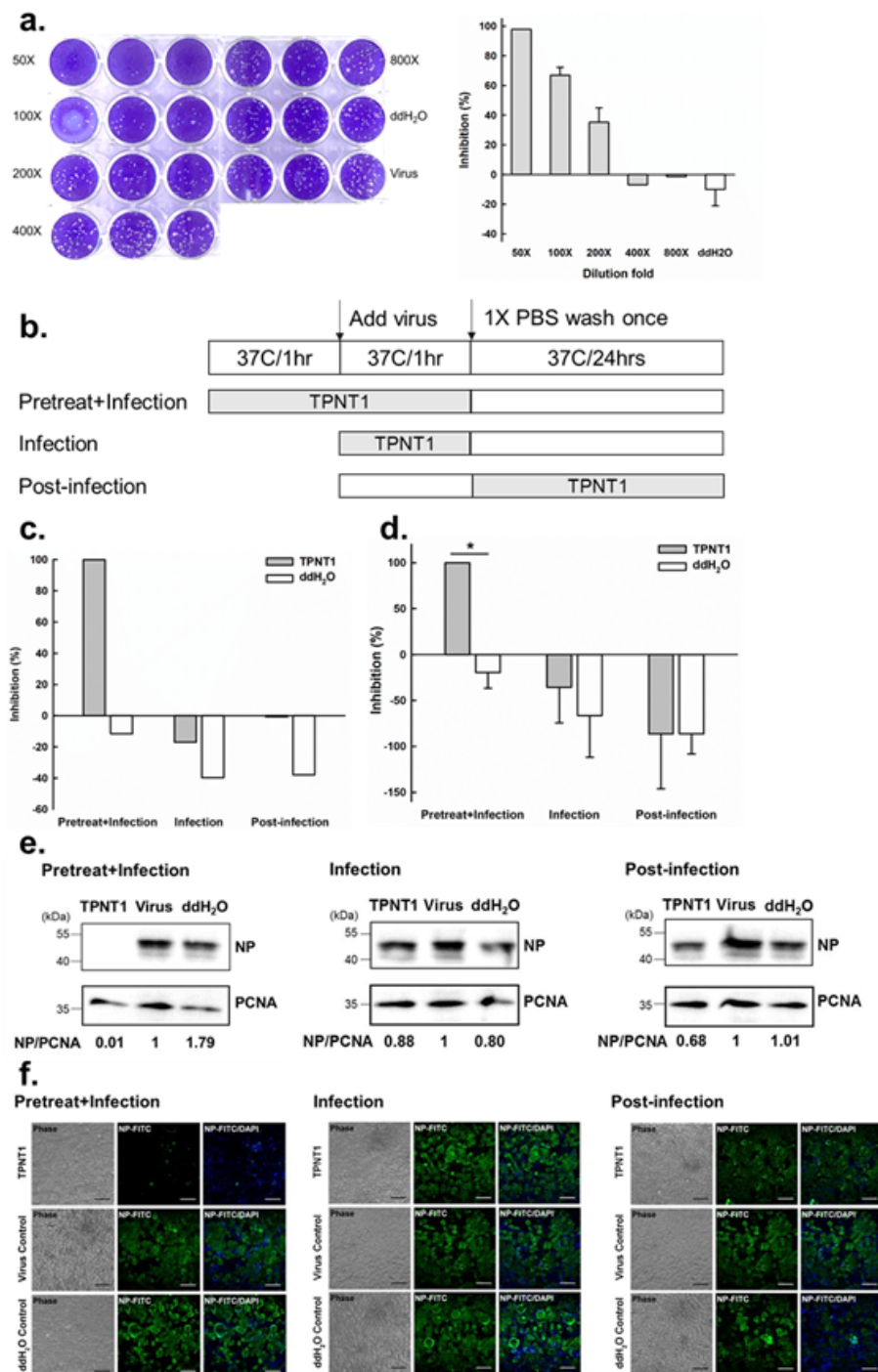
Figures

Figure 1

The antiviral activities of TPNT1 against SARS-CoV-2 in vitro. A. Plaque reduction assay was performed to determine the antiviral activity of TPNT1 against SARS-CoC-2. Briefly, the virus was incubated with TPNT1 at 37°C for one hour before adding to the Vero E6 cells. After virus infection, the cells were washed once with PBS buffer and then overlaid with medium containing 1% methylcellulose. The cell culture was maintained at 37°C for 5–7 days before fixation with 10% formalin and stained with 0.5%

crystal violet. The percentage of inhibition was calculated as [1 − (VD / VC)] × 100%, where VD and VC refer to the virus titer in the presence and absence of the test compound, respectively. ddH2O was used to prepare serial dilution of TPNT1 and was used as solvent control. B−F. Yield reduction assay was conducted to evaluate the stages that TPNT1 exerts its antiviral activities against SARS-CoV-2. Schematic illustration of the pretreat + infection, infection-only, and post-infection experiments delineates the stage where TPNT1 was added to the viruses or the cells (B). Briefly, the virus (multiplicity of infection, M.O.I. = 0.01) was pretreated with TPNT1 and was added to the Vero E6 cells (pretreat + infection), or TPNT1 was added during (infection) or after virus infection (post-infection). After virus infection, the cells were washed once with PBS, and the cells were maintained in medium with or without TPNT1 for 24 h. The viral copy numbers in the culture supernatant was quantified by qRT-PCR (C). The viral nucleocapsid (NP) protein and viral RNA expression in the SARS-CoV-2 infected Vero E6 cells was determined by western blot (D) and qRT-PCR detection of oligo-dT amplified cDNA (E). The expression of viral nucleocapsid proteins (NP) upon treatment of TPNT1 at different stages was also determined by immunofluorescence staining (F). The infected cells from yield reduction assay were fixed, and then probed with a rabbit monoclonal antibody against the NP of SARS-CoV 2 (1:200; 40103-R019, Sinobiological, China) and FITC-labeled goat anti-rabbit IgG (1:300; Jackson ImmunoResearch, USA). The nuclei were stained with DAPI. The Infection and post-infection experiment shared the same virus control well. Scale bars: 100 μm.
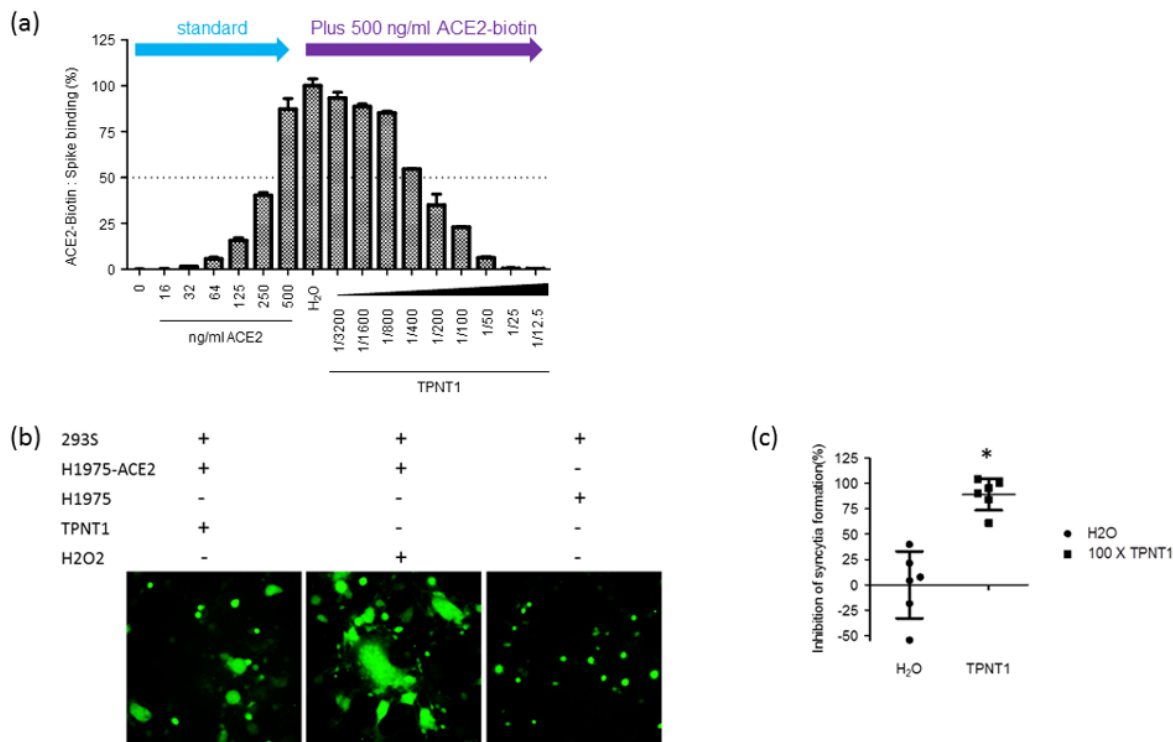

Figure 2

Inhibition of SARS-CoV-2 entry by TNPT1. (A) The inhibition of SARS-CoV-2 spike protein binding to ACE2 in the presence of different concentration of TPNT1 was determined by the ELISA assay. (B) The ability

of TPNT1 to inhibit the syncytium formation, a step critical for virus entry after receptor binding, was demonstrated by the syncytia assay.
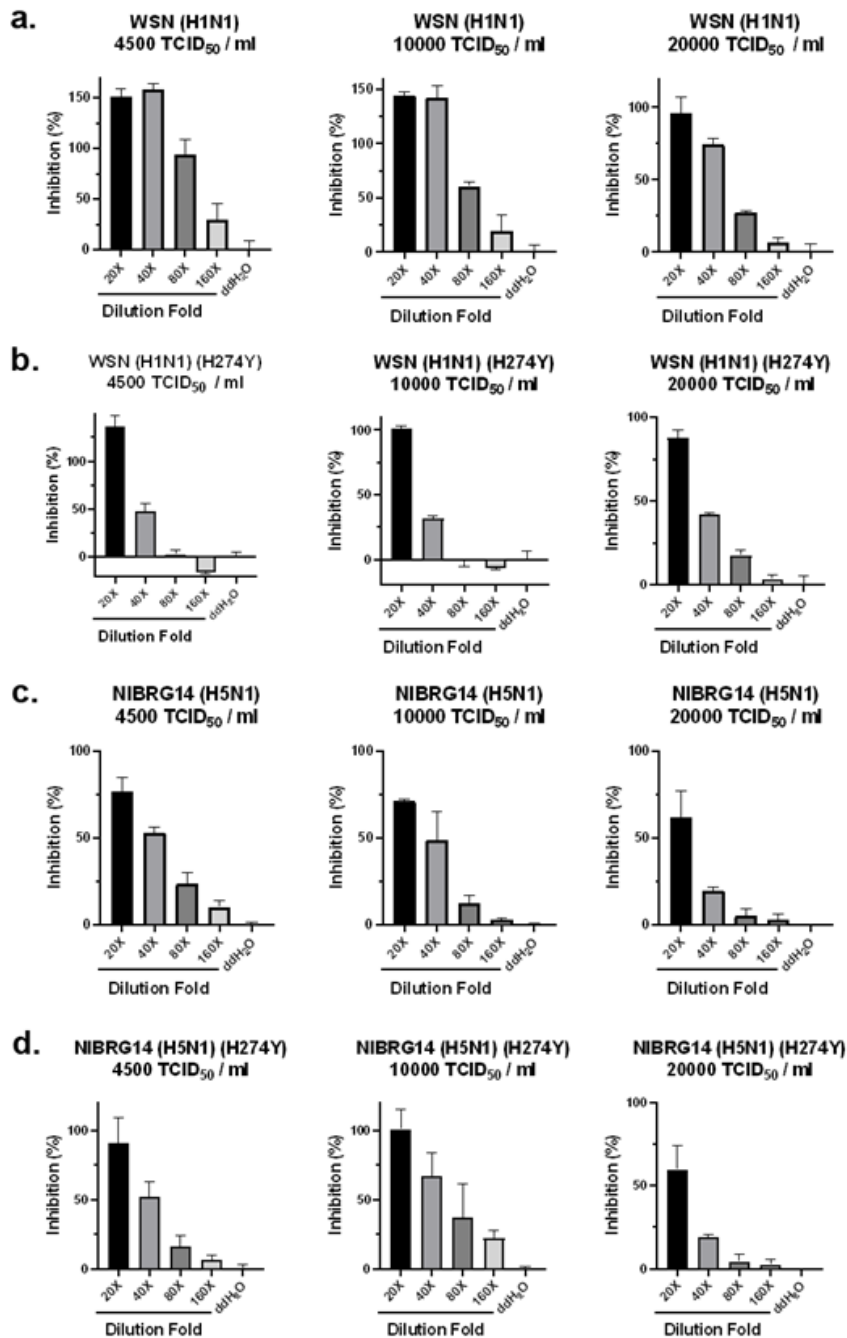

Figure 3

The antiviral activities of TNPT1 against influenza viruses in vitro. MDCK cells were incubated with WSN (H1N1) (A), drug-resistant WSN (H1N1)(H274Y) (B), NIBRG14 (H5N1) (C), and drug-resistant NIBRG14 (H5N1)(H274Y) (D) at various viral loads in the presence of TNPT1. After 48 h at 35 °C, the virus-induced

cytotoxicity was monitored. The cells incubated with virus only were defined as 0% while the cells with no virus incubation were defined as 100% inhibition.

Supplementary Files

This is a list of supplementary files associated with this preprint. Click to download.

- SFig1.tif
- SFig2.tif
- SFig3.tif